

# Grooving an alumina surface as a mean to inhibit secondary electron emission under grazing incidence

J. Guéna, E. Jahier, M. Lintz, A. Papoyan\*, S. Sanguinetti, M.A. Bouchiat

*Laboratoire Kastler Brossel<sup>†</sup>, Département de Physique de l'Ecole Normale Supérieure,*

*24 Rue Lhomond, F-75231 Paris Cedex 05, France*

*e-mail: marianne@lkb.ens.fr*

(11 september 2002)

## ABSTRACT

We observe charge multiplication of photoemitted electrons in cylindrical alumina cells, containing cesium vapor, submitted to a longitudinal electric field and to intense laser pulses. We present several diagnosis allowing us to attribute this charge multiplication to efficient secondary electron emission (SEE) from the accelerated photoelectrons colliding with the inner wall at grazing incidence. Machining mm-size triangular grooves on the initially smooth inner wall, so as to prevent grazing incidence, is shown to be efficient in reducing SEE. The atomic signal characteristic of the space charge accumulated close to the anode is found to be reduced by more than one order of magnitude. This result is of important significance, not only for our Parity Violation experiment in cesium vapor (Eur. Phys. J. D **13** (2001) 221), but also for experiments and techniques involving SEE at grazing incidence.

**PACS.** 79.20.Hx Electron impact : secondary emission - 33.55.b Optical activity and dichroism : magneto-optical and electro-optical spectra - 39. Instrumentation and techniques for atomic and molecular physics.

## INTRODUCTION

Secondary Electron Emission (SEE) is a very general mechanism taking place when a surface is irradiated by any kind of incident particle [1,2]. Microchannel plates [3] used for detection of photoelectrons or X Ray photons fully benefit from SEE; but in several applications SEE actually turns out to be troublesome. Many surface analysis techniques make use of ionizing particles where SEE can be a serious complication because electronic emission necessarily results in a change of the surface potential of insulating materials. This not only affects the spectroscopy of the signals detected, but can even deviate the incident beam of charged particles [2]. The secondary electrons colliding with the wall often cause outgassing and surface conditioning is required [4]. In high energy proton accelerators, where synchrotron irradiation can be strong, photoelectrons emitted by the walls are accelerated by the positively charged proton bunches and collide with the wall, giving rise to an “electron cloud” of secondaries and to an instability of the trajectories of the proton bunches [5]. In RF fields, accelerated secondaries can produce “multipactor” effects [6] leading to damage (breakdown and melting) of the dielectric windows used in high-power klystrons [7]. In our Parity Violation (PV) experiment [8,9], where an electric field has to be applied along the axis of a cylindrical dielectric vapor cell, SEE has an important bearing upon the experimental conditions, in particular the electric field map. This can be a source of systematic effects. This paper presents a solution found to strongly reduce the occurrence of SEE on the wall of the cell.

We begin with a short presentation of the experiment (Sec. I). Next (Sec. II), we indicate what kinds of diagnosis have led us to attribute to SEE the observed perturbations. Our solution to this problem and the improvement obtained are described in the last section (Sec. III).

---

\*permanent address: Institute for Physical Research, Ashtarak-2, 378410 Armenia

<sup>†</sup>Laboratoire de l'Ecole Normale Supérieure associé au CNRS (UMR 8552) et à l'Université Pierre et Marie Curie

## I. EXPERIMENTAL CONDITIONS AND METHODS

### A. Set-up

Our experiment is performed on Cs atoms in a vapor contained inside a cylindrical cell submitted to laser light pulses and an electric field along the common axis of the cell and light beam. The set-up is the same as we use for our ongoing PV experiment in atomic cesium, described in detail in [9]. We give only a brief description of the part relevant for the present work. The body of the cell<sup>1</sup> consists of a tube ( $L= 83$  mm,  $\varnothing_{int} = 10$  mm,  $\varnothing_{ext} = 13$  mm) made either of monocrystalline  $\alpha$ - $\text{Al}_2\text{O}_3$  (sapphire) or (99.7% purity) alumina ceramics, with two sapphire windows (thickness, 0.5 mm) glued at the ends. A side arm glued in the middle of the main tube contains a few  $\text{mm}^3$  of liquid cesium. The body of the cell is placed between annular electrodes 1 cm apart [10], inside an oven heated up to  $350^\circ\text{C}$ . Thanks to the side-arm, the cesium droplet can be kept at a much lower temperature, in the range  $140$ - $150^\circ\text{C}$ , to yield Cs vapor with atom number density in the range of  $1$  to  $2 \times 10^{14}$   $\text{cm}^{-3}$ . The oven has small orifices for the passage of laser beams. The longitudinal electric field is produced by applying to the electrodes high voltages growing by steps from  $-V_0$  to the first electrode to  $+V_0$  to the last electrode ( $V_0 \simeq 10$  kV). The geometry of the electrodes and insulators around the cell has been optimized so as to ensure homogeneity of the longitudinal field component in the interaction region (of radius of 0.7 mm centred around the axis) to better than  $10^{-3}$  rms and transverse components not exceeding  $10^{-3}$  rms [10]. The electric field can be reversed with a symmetry better than  $5 \times 10^{-3}$ , a feature useful for diagnosis. In order to avoid discharges in Cs vapor the high voltages are applied as pulses of duration of  $\sim 200$  ns, the 20 ns laser pulses being sent through the cell during the electric field plateau. Typical repetition rate is 100 Hz.

### B. Space charge diagnosis and measurements

For atomic diagnosis of electron emission, as for the PV measurements, we tune the intense 539 nm laser beam to resonance with the forbidden 6S–7S transition of Cs atoms. We exploit the sensitivity of this transition to an electric field  $\vec{E}$  via Stark mixing between S and P states. The Stark induced transition excited by a resonant light beam of wave vector  $\hat{k}$  is described by a transition dipole between the atomic 6S and 7S states [8],

$$\vec{d}_{6S-7S}^{Stark} = -\alpha\vec{E} - i\beta\sigma \times \vec{E} + M_1\sigma \times \hat{k}, \quad (1)$$

where  $\alpha$  and  $\beta$  are the scalar and tensorial transition polarizabilities ( $\beta \simeq \alpha/10$ ),  $M_1$  is the magnetic dipole amplitude ( $M_1/\alpha \simeq 3$  V/cm), and  $\sigma$  is the electronic spin operator. As one can see from the above expression, the transition dipole can be used to analyze the direction of the  $\vec{E}$  field. Population, orientation and alignment are created in the 7S state with specific contributions depending on the laser polarization  $\hat{e}$  (linear or circular) and the direction of the electric field. To probe the 7S state we use a second laser beam colinear to the exciting beam, which is tuned to resonance with a single hyperfine component of the 7S– $6P_{3/2}$  transition (near  $1.47$   $\mu\text{m}$ ). The transmitted intensity of the probe is amplified and its polarization is modified. Monitoring these effects allows us to measure the 7S population and the angular momentum anisotropy of the 7S state by using highly sensitive differential polarimetry [12]. Such anisotropy measurements can reveal the presence of *transverse components of the electric field* which would be absent, were the real electric field as homogeneous as the numerical simulation predicts ( i.e. if the electric field map were given only by the potentials applied to electrodes and the dielectric properties of the insulators). In the present paper we are interested in those components which manifest the presence of free charges inside the cell.

Any transverse field is easily detected because the corresponding Stark-induced amplitude,  $\vec{d}_{6S-7S}^{Stark} \cdot \hat{e}$ , interferes with the one induced by the longitudinal field  $E_z$ . This results in a 7S alignment which, after precession in a suitable magnetic field, is detected as a linear dichroism for the probe beam, averaged over the volume and the laser pulse duration [12]. The transverse electric field appears to be small or zero near the axis of the cell (as expected from symmetry considerations), and increases radially, as  $|\vec{E}| \propto r$ , when the pump and probe beams are translated away from the centre (Fig. 1). This radial field  $\vec{E}_{rad}$  does not change sign when the applied electric field is reversed: it is a *centripetal field* which indicates that a distribution of *negative charges* fills the cell (see Fig. 1). It appears to saturate at an excitation laser energy density as low as  $\sim 0.05$  mJ/mm<sup>2</sup>, while we operate with typically 0.6 mJ/mm<sup>2</sup> for PV

---

<sup>1</sup>constructed by D. G. Sarkisyan's group at Institute of Physical Research, Ashtarak, Armenia [11].

measurements. We actually found little difference on the magnitude of  $E_{rad}/r$  at saturation in four cells of identical geometry but different materials : sapphire of different origins for three of them, and alumina for the last one, polished using different procedures. Typical values of  $E_{rad}/r$  are 25 to 45 V/cm/mm in sapphire cells and 28 V/cm/mm in the 99.7% alumina cell<sup>2</sup>. From Gauss' law, the negative charge density is estimated to be  $\sim 2.5$  to  $4.5 \times 10^8$  elementary charges per  $\text{cm}^3$ .

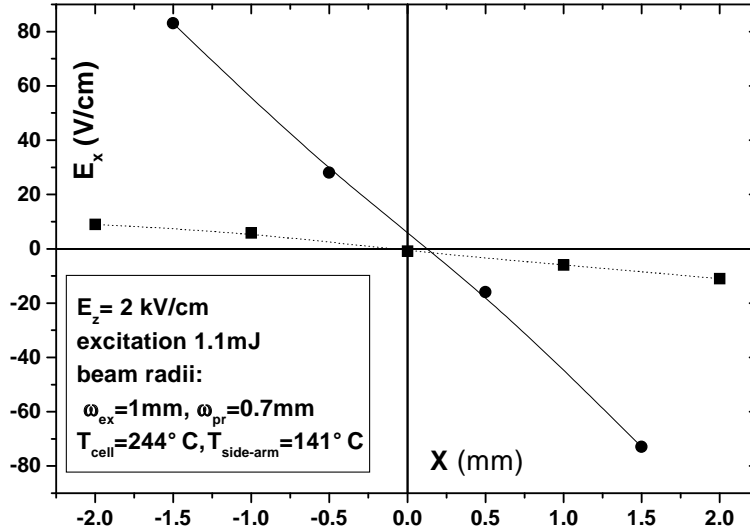


FIG. 1. Transverse electric field component  $E_x$  observed when the excitation and probe beams, while kept superposed, are translated in the transverse  $x$  direction of the cell. Circles: smooth-wall sapphire cell and squares: grooved-wall alumina cell. Similar behavior is observed for  $E_y$  for translation along  $y$ . The  $x=0$  position defined mechanically is arbitrary to within 0.5 mm.

We were able to study the charges in more detail because we detect an atomic signal indicating the presence of an orthoradial magnetic field [13]. The existence of such a field indicates that the charges flow through the cell. The flow velocity, deduced from the B-field magnitude, appears compatible with what is expected for charges of mass  $m_e$ , hence electrons, driven by the applied electric field from one window to the other in only 2 ns. Taking into account the volume of the cell, the transit time and the laser pulse duration, we can evaluate that  $\sim 4 \times 10^{10}$  charges per pulse flow through the cell. This clearly means a large current and Sec. II shows how current measurements provided a clue to our understanding of the process involved.

## II. MANIFESTATIONS OF SECONDARY EMISSION

### A. Direct current measurements

For the electron current measurements we use the fact that the high value of the dielectric constant of sapphire ( $\epsilon=11.8$ ) gives rise to a strong capacitive coupling between the two sides of a 0.5 mm thick sapphire window. If the outer sides of the windows are coated with a conductive material and connected to the HV supply, the current pulse of the electrons reaching (leaving) the anode (cathode) window induces an equivalent current pulse from the HV supply. The latter pulse can be easily measured, for instance using a pulsed current transformer (“Rogovski coil”).

<sup>2</sup>AL23, 99.7% alumina ceramics from Degussa-Huls.

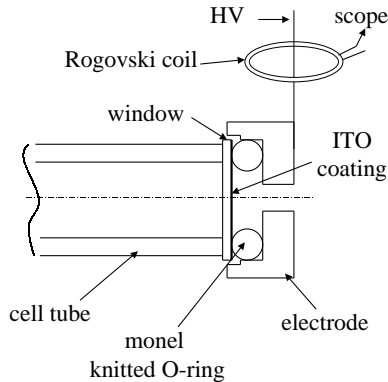


FIG. 2. Schematic of the electrical contact between the ITO-coated window and the nearby end electrode. Both beam and E-field axes are along that of the cell tube.

The conductive coating of the sapphire windows was obtained by a 160 nm indium-tin deposition in vacuum followed by oxidation in air at 300°C for 4 hours. The indium tin oxide (ITO) layer is conductive (square resistance 100  $\Omega$ ) and transparent at both wavelengths ( $T > 0.85$ ). Connection to the HV supply is made by a Monel (40% Cu, 60% Ni) knitted and flexible O-ring, pressed between the coated window and the outermost electrode (Fig.2).

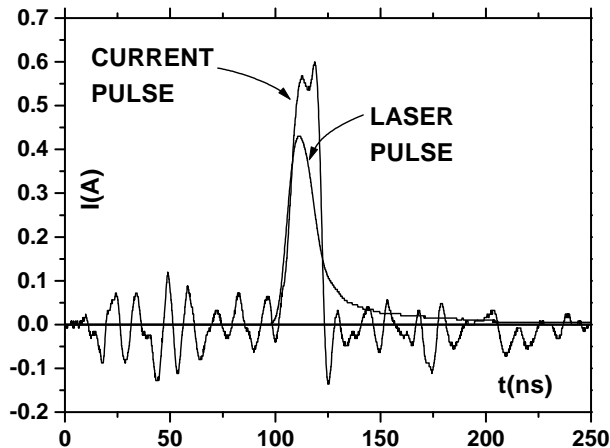


FIG. 3. Current pulse induced by the 539 nm-laser pulse, measured (see Fig 2) at the anode window. The HV plateau starts at  $t=0$ . Two recordings, with then without a laser pulse, were used to subtract the HV charge (and discharge) current. (HV=9 kV; laser pulse energy is 0.7 mJ). The current pulse size is compatible with the magnitude of  $E_{rad}$  measured in the same cell (dots in Fig. 1). At the cathode window no current pulse could be observed.

The latter is connected to the HV supply by a wire in which we measure the current using a Pearson Rogovskii coil (model 2878: 5 ns rise time, sensitivity 0.1 V/A). Without laser pulses in the cell, we measure pulses corresponding to the charge and discharge of the electrodes at the beginning and at the end of the electric field plateau. This allows us to check the voltage-to-current calibration of the Rogovskii coil and the signs of the current pulses. With a 539 nm laser pulse sent during the HV plateau, we can measure on the anode side a positive current pulse from the HV supply, of the order of 0.6 A in typical conditions, during the  $\sim 20$  ns of the laser pulse (see Fig. 3). This indicates that  $8 \times 10^{10}$  electrons have reached the anode window. This number of charges is compatible with that we have extracted from the magnitude of the radial field gradient averaged over  $z$  and  $t$  (Sec. I B). By contrast, the current pulse measured at the cathode window is barely detectable, i.e. smaller by at least one order of magnitude. Since the charge reaching the anode is considerably larger than that leaving the cathode, we conclude that a multiplication of the electron charge occurs. The likely origin is SEE due to primary electrons, photoemitted at the cathode window (see Sec. 5 in [14]), accelerated by the longitudinal  $\vec{E}$  field and colliding at grazing incidence against the tube wall. Indeed we have calculated the average radial motion of an electron photoemitted at the window, which moves in the

radial electric field generated by the preceding electrons. We take into account i) the initial transverse velocity of the electrons, preferentially emitted along the linear light polarization, and their kinetic energy  $h\nu - W$ , where  $W \simeq 1.4$  eV is the work function of the cesiated  $\text{Al}_2\text{O}_3$  surface [14] and  $h\nu = 2.3$  eV at 539 nm, ii) the force exerted by the other electrons, evaluated from the measured radial field, iii) the radius of the emitting area over which photoemission exceeds or reaches saturation: 1.2 mm. We find that a significant fraction of the emitted primaries have a chance to hit the tube wall before reaching the window. On the other hand, primary photoemission on the tube wall, due to stray light, is unlikely, owing to high optical quality of the window and the absence of illumination on the cell body.

### B. Manifestation via a highly sensitive atomic signal

Since we observe that an important charge flow transits through the cell and reaches the anode, and since even 15 keV electrons do not penetrate sapphire by more than a few  $\mu\text{m}$ , those charges are necessarily stopped at the anode window and cause a locally important drop of the longitudinal  $E_z$  field magnitude at this extremity of the cell. We have looked to probe such an effect via some atomic signal. At first sight, the pump-probe configuration of our experiment does not look favorable for detecting inhomogeneities of the electric field along the beam propagation direction  $\hat{k}$ , since any property of the probe beam integrates the atomic effects over the whole column length of the irradiated vapor. However, as shown below, there are means of overcoming such a difficulty.

The basic idea is that the 7S atomic density  $n_{7S}(z)$  at each position of coordinate  $z$  is proportional to  $|E_z(z)|^2$ . By choosing properly the physical observable detected, we are free, to some extent, to assign different weights to atomic contributions located at different  $z$  positions. If, for instance, a longitudinal magnetic field is applied, the probe detects an optical rotation of the vapor,  $\propto \int E_z(z)^2 B(z) dz$ , whose sign reverses with the  $\vec{B}$  field direction [15]. For one particular transition,  $6S_{1/2, F=3} \rightarrow 7S_{1/2, F=4} \rightarrow 6P_{3/2, F=5}$ , the sensitivity is high : 200 mrad/G in a homogeneous magnetic field. For diagnosis, we apply a  $\vec{B}$ -field *gradient*, characterized by opposite values of the field close to the input and output windows. We expect the electric field drop to take place close to the anode, that is at the input or at the output of the cell, depending on whether  $\vec{E}$  is colinear or anticolinear with  $\hat{k}$ . Therefore, *the Faraday effect acquires a contribution which is odd under electric field reversal* and linear in the magnetic field gradient. We have indeed observed such an effect, with the expected sign, when applying a field difference  $B_z^{in} - B_z^{out}$  as small as 13 mG. This confirms that an electron space charge accumulates at the anode as a result of charge multiplication by SEE.

We may remark that this effect exactly simulates the Faraday effect induced by a homogeneous magnetic field component which would truly reverse with the electric field,  $B_z(E_z \text{ odd})$ , hence the denomination of a pseudo field  $B_z^{pseudo}(E_z \text{ odd})$ . A natural parameter for evaluating the  $E(z)^2$  inhomogeneity is actually the ratio of the measured pseudo field to the applied field difference  $B_z^{in} - B_z^{out}$ , i.e.  $\rho = B_z^{pseudo}(E_z \text{ odd}) / (B_z^{in} - B_z^{out})$ . In this ratio the Faraday constant for the chosen atomic transition is eliminated. In cells tested, we found  $\rho = 1/17$  for sapphire tubes and  $1/28$  for the alumina tube. In the particular ITO-coated cell (Sec. II.A), although  $\rho$  was substantially smaller than before ITO coating<sup>3</sup>, it exhibited large temporal variations.

True or pseudo fields  $B_z(E_z \text{ odd})$  are dangerous sources of systematics in our PV experiment<sup>4</sup>. If, in addition, they are unstable, then one cannot correct for them. Hence, smallness and stability of those fields are essential for achieving precise PV measurements. How we dealt with this problem is discussed in the following section.

### III. REDUCTION OF SECONDARY ELECTRON EMISSION

General features of SEE are given in the literature [1]. It is found that the SEE efficiency in insulators is larger than in metals, when irradiated under the same experimental conditions. In a metal, a secondary loses its energy in collisions with conduction electrons, whereas in insulators the contribution of bound electrons is hindered by the high gap value: only lattice vibrations and imperfections contribute to the collision rate of secondary electrons. The SEE yields (ratio of secondary to primary current) have been measured at normal incidence with a scanning electron microscope [6]. In  $\text{Al}_2\text{O}_3$  (9.4 eV energy gap), they are larger than unity:  $\sim 2$  for 99.7 % alumina and  $\sim 4$  for sapphire in the 10–20 keV

<sup>3</sup>As expected, application of the electric field via a conductive coating right on the outer side of the 0.5 mm sapphire window ( $\epsilon = 11.8$ ) is more efficient against perturbing charges than application via the outer ring electrodes several mm away.

<sup>4</sup>They can simulate the PV effect when their magnitude reaches 50  $\mu\text{G}$ .

energy range, relevant here. At lower energy they reach  $\sim 10$  for sapphire. Moreover, cesium adsorption, inducing a  $\sim 2$  eV drop of the  $\text{Al}_2\text{O}_3$  work function from 3.3–3.7 eV [16] to 1.35–1.45 eV [14] in the presence of Cs vapor, strongly favors SEE by lowering the escape barrier<sup>5</sup>. It has been reported that SEE efficiency depends on incidence: it is higher at grazing incidence, because the secondary electrons are produced very close to the surface and have a large escape probability (see for instance [18]). It is also known that energetic electrons propagating in matter have a peak of the differential ionization cross-section in the forward direction. In our experimental configuration, grazing incidence definitely looks harmful.

Considering that, among the three factors - wall material, Cs adsorption, and grazing incidence - only the latter could be easily and efficiently used to lower the SEE yield, we decided to replace the smooth internal surface of our sapphire and alumina cells by a grooved surface preventing electrons from colliding at tangential incidence. For the PV experiment it is important to preserve revolution symmetry, as well as the  $z/z$  reflexion. This was made by machining regular circular grooves inside an alumina tube, as shown on Fig. 4. Only the central part of the tube (over a length of  $\sim 4$  mm) was left smooth in order not to complicate gluing of the side arm. Machining made use of a sharp tool of  $60^\circ$  tip angle, penetrating inside the alumina over a depth of 0.87 mm. The tool is translated by steps of 1.0 mm. This procedure avoids the presence of flat tops or finite machining radius at the top of the grooves but leaves from place to place some tiny broken facets, oriented randomly. The typical groove dimension (here chosen to be 1 mm for practical reasons linked to the machining) is not critical. Smaller dimensions should give similar results. Basically the grooves act as a succession of screens, provided their thickness is much larger than the mean free path of the secondary electrons. By contrast, nm-size roughness does not inhibit and in some circumstances even enhances SEE [19].

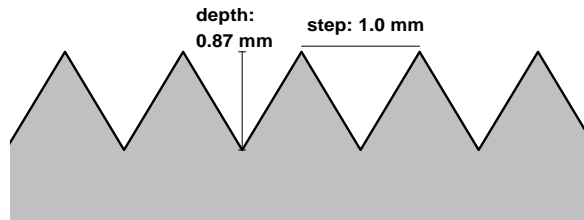


FIG. 4. Profile of the grooves machined on the inner wall.

The new cell differed from previous alumina cells only by grooving at the internal surface. With it, we repeated the atomic measurements described in section II.B. We found a  $\rho$  factor consistent with zero at the statistical level of 1/300, i.e. more than one order of magnitude less than the value in smooth-wall cells. We also found that the radial centripetal field,  $\vec{E}_{rad}$ , was reduced substantially, as exhibited in Fig. 1, although less than the  $B_z^{pseudo}(E_z \text{ odd})$  field. This is understandable if we note that  $\vec{E}_{rad}$  involves the charge density averaged over the whole length of the tube, while  $B_z^{pseudo}(E_z \text{ odd})$  mostly involves the charges accumulated at the anode window.

Another notable observation concerns the value of the  $E_z \text{ odd}$  contribution to the Faraday effect *without any applied magnetic field or any B field gradient*. This effect informs us about the existence of a true  $E_z \text{ odd}$  component of the magnetic field,  $B_z(E_z \text{ odd})$  which, given the symmetry of the experiment, should be absent. Actually, in all cells with smooth surface tube we observed a non-zero  $B_z(E_z \text{ odd})$ , sometimes irreproducible in magnitude, with typical values in the range 100 –200  $\mu\text{G}$ . In the new cell with grooved walls, after averaging, the  $B_z(E_z \text{ odd})$  field is found compatible with zero at the level of 5  $\mu\text{G}$  (present statistical uncertainty). The most likely origin that we can suggest for this field is associated with the photoinduced current which flows through the cell during the excitation pulse<sup>6</sup>. In smooth-wall cells this current reaches a fraction of Ampere (see Fig. 2). We can explain the observed  $B_z(E_z \text{ odd})$

<sup>5</sup>In the case of diamond, SEE enhancement factors of more than one order of magnitude have been observed due to Cs adsorption [17].

<sup>6</sup>Several other interpretations, involving for instance charge motion in residual magnetic fields or mechanical imperfections of the HV connections to the electrodes, have been considered, tested and rejected as leading to too small effects [13].

field if this current is inhomogeneously distributed (due to inhomogeneous SEE properties of the tube surface) and a fraction as small as a few thousandths happens to become equivalent to a coil of  $z$ -axis. In other words, the surface inhomogeneities of the tube can generate a chiral contribution to the photoinduced current having a fluctuating amplitude, and even sign, when the tube temperature or excitation energy vary. This interpretation appears to be well supported by our observation reported above, that the effect is considerably reduced with a grooved surface which strongly reduces SEE.

## CONCLUSION

In our experimental configuration with a longitudinal electric field, where the electrons propagate nearly parallel to the wall and hit them under grazing incidence, we have demonstrated directly a large multiplication of electrons between the cathode window, where they are photoemitted, and the anode window where they stop. Moreover, we have found a sensitive atomic signal manifesting that same effect. Based on the measured atomic signal, we have concluded that one can reduce SEE significantly merely by changing the physical state of the wall, i.e. by changing it from smooth to grooved in order to make collisions at tangential incidence unlikely. Such a result has a direct impact on the advancement of our PV experiment since by this technique we can suppress a hitherto troublesome  $B_z(E_z \text{ odd})$  magnetic field component.

Note added: Owing to the progress allowed by the work presented here, we have now observed with 10% accuracy [20], with the expected sign and magnitude ( $10^{-6}$ ), the chiral amplification of the probe manifesting Parity Violation in our pump-probe configuration [9,10].

The authors thank Ph. Jacquier and M.D. Plimmer for helpful discussions and careful reading of the manuscript. We are grateful to D. Sarkisyan for special care taken during the construction of several alumina cells.

- 
- [1] Encyclopaedic Dictionary of Physics, ed. J. Thewlis, (Pergamon Press, Oxford, 1962), Vol.6.
  - [2] J. Cazaux, in *Ionization of Solids by Heavy Particles*, ed. R.A. Baragiola, NATO ASI Ser. B **306**, 325 (Plenum Press, New York, 1993).
  - [3] <http://hea-www.harvard.edu/HRC/mcp/mcp.html>
  - [4] O. Gröbner, Abstract of the Summary of the talks on Secondary electron emission, [www.aps.anl.gov/conferences/icfa/papers/grobner-sum.pdf](http://www.aps.anl.gov/conferences/icfa/papers/grobner-sum.pdf)
  - [5] <http://www.slac.cern.ch/collective/electron-cloud/>
  - [6] Y. Saito, S. Michizono, T. Sato, S. Kobayashi and C. Jardin, in *Proceedings of the Third Int. Conf. on Electric Charge in Solid Insulators*, ed. G. Dammane (SFV, Paris 1998).
  - [7] S. Michizono, Y. Saito, S. Yamaguchi, S. Anami, N. Matuda and A. Kinbara, IEE Transactions on Electrical Insulation, **28**, 692 (1993).
  - [8] M. A. Bouchiat and C. Bouchiat, *Rep. Prog. Phys.* **60**, 1351 (1997).
  - [9] J. Guéna, D. Chauvat, Ph. Jacquier, M. Lintz, M. D. Plimmer and M. A. Bouchiat, *Quantum Semiclass. Opt.* **10**, 733 (1998).
  - [10] E. Jahier, J. Guéna, Ph. Jacquier, M. Lintz and M. A. Bouchiat, *Eur. Phys. J. D* **13**, 221 (2001).
  - [11] D. G. Sarkisyan, A. V. Melkonyan, *Instr. and Exp. Techn.* **32**, 202 (1989)
  - [12] J. Guéna, D. Chauvat, Ph. Jacquier, M. Lintz, M. D. Plimmer and M. A. Bouchiat, *J. Opt. Soc. Am. B* **14**, 271 (1997); M. A. Bouchiat, D. Chauvat, J. Guéna, Ph. Jacquier, M. Lintz and M. D. Plimmer, *Opt. Commun.* **119**, 403 (1995).
  - [13] E. Jahier, Thèse de l'Université Paris VI, 2001 ([http://theses-en-ligne.in2p3.fr/view-thes-phys-atom\\_fr.html](http://theses-en-ligne.in2p3.fr/view-thes-phys-atom_fr.html))
  - [14] A. Papoyan, J. Guéna, M. Lintz and M. A. Bouchiat, *Eur. Phys. J. AP* **19**, 15 (2002).
  - [15] M. A. Bouchiat, J. Guéna, Ph. Jacquier, M. Lintz and M. D. Plimmer, *Z. Phys. D* **33**, 89 (1995).
  - [16] M. Brause, D. Ochs, J. Gunster, Th. Mayer, B. Braun, V. Puchin, W. Maus-Friedrichs, and V. Kempter, *Surf. Sci.* **383**, 216 (1997) and V. Kempter, private communication.
  - [17] J. Cazaux, *J. Appl. Phys.* **89**, 8265 (2001).
  - [18] M. Salehi and E. A. Flinn, *J. Appl. Phys.* **52**, 994 (1981).
  - [19] Y.C. Yong, J.T.L. Thong and J.C.H. Phang, *J. Appl. Phys.* **84**, 4543 (1998).
  - [20] arXiv: physics/0210069